Networked Salt-Bridges Mediate Magnesium-Dependent Conformational Dynamics and Functional Regulation in Type IA Topoisomerases

Yeonee Seol[1], Yuk-Ching Tse-Dinh[2], Keir C. Neuman[1]*

*Corresponding author: neumankc@nih.gov

The PDF file includes:

Supplementary Text
Extended Data Table 1
Extended Data Figs. 1 to 15
References 1-10

Supplementary Text

Magnesium dependent *ec*topo3 DNA cleavage and religation

To obtain the magnesium-dependent ssDNA cleavage and religation kinetics, we first generate a covalent enzyme-DNA cleavage complex by incubating negatively supercoiled plasmid with *ec*topo3 in the absence of magnesium, which supports cleavage but not religation. We then measure the reduction in cleaved DNA over time under different magnesium concentrations (Extended Data Fig. 2A), from which the cleavage and ligation kinetics, and equilibrium can be obtained. In detail, enzyme-DNA covalent cleavage complexes were prepared by incubating DNA with *ec*topo3 at 37°C for 30 min (900 nM negatively supercoiled pBR322 and 18 µM enzyme in 20 µl of topoisomerase buffer supplemented with 1 mM EDTA to prevent religation after cleavage). 10 µl of the enzyme-DNA cleavage complex was pipetted into each tube containing 90 µl of topoisomerase buffer with different $MgCl_2$ concentrations (0, 0.3, 3, and 10 mM) preequilibrated at 37°C. For each time point (0, 15, 30, 60, 150 and 300 s) 10 µl from each of the 4 different $MgCl_2$ concentrations was transferred to a new tube containing 1 µl of 10% SDS and 4 units of Proteinase K for inactivation. Inactivation was performed at 42°C for 2 hours. The religation samples were run on a 1% agarose gel for 2 hours at 80V. The gel was stained with Sybrgold and the image was analyzed with Fiji to quantify the cleaved DNA bands on the gel for each condition [1].

The change in the cleaved DNA over time was fit with Eq. s1 (Extended Data Fig. 2A top).

$$[C] \underset{k_C}{\overset{k_L}{\rightleftarrows}} [L];$$

$$\frac{d[C]}{dt} = k_C[L] - k_L[C]; [L] = [total\ DNA] - [C]\ ;$$

$$\frac{[C]}{[total\ DNA]} = \frac{k_L}{k_C+k_L}\exp(-(k_C + k_L)t) + \frac{k_C}{k_C+k_L} \qquad \text{Eq. s1}$$

$$K_{L/C} = \frac{k_L}{k_C}$$

$[C]$ indicates the cleaved DNA concentration and $[L]$ is the ligated DNA concentration. k_C and k_L are the cleavage and religation rates respectively. k_C, k_L, and the religation and cleavage equilibrium, $K_{L/C}$ for different Mg^{2+} were obtained from the fits (Extended Data Fig. 2B).

Single-stranded DNA binding affinity measurements using fluorescent polarization anisotropy (FPA)

FPA measurements were performed with 5′ fluorescein labelled dT55 single-stranded DNA. Using a 96 well plate, varying enzyme concentrations (0 – 8 nM) and Mg^{2+} concentrations (0 – 10 mM) in topoisomerase buffer (20 mM Tris, pH adjusted to 8.0, 100 mM potassium glutamate, and 1mM Dithiothreitol) were added to individual 96 wells containing 2 nM ssDNA and the reactions were incubated at room temperature for 30 min prior to the measurement. Measurements were repeated three times.

Statistical analysis of SMD simulations to estimate the gate opening transition probabilities and the average waiting times prior to gate opening

For simplicity, we assume that the protein gate opening transition is a single energy barrier crossing event, which results in an exponential waiting time distribution with an average rate, λ. The average rate can be significantly overestimated if the waiting times for the simulations with opening transitions are considered to obtain the opening rate estimate since many of the simulations end before the gate opens. If the simulation durations are all the same, Tm, then the average probability of opening in a simulation duration is $\overline{p}$:

$$\overline{p} = \int_0^{Tm} \lambda \exp(-\lambda t)\ dt = 1 - exp(-\lambda Tm)$$

Thus, we can estimate the rate of opening by determining the average probability of opening in the simulation time *Tm*. Given this average probability of opening for each simulation, individual simulations can be treated as a Bernoulli trial with opening probability *p* and the probability of observing *k* openings in *n* simulations can be described with the binomial probability mass function.

Based on Bayes's theorem, the posterior conjugate of the binomial likelihood is a beta distribution [2]. Setting the beta uniform distribution β (1, 1) as a conjugate prior, the gate opening probability density distribution is calculated as:

$$PDF\ (p;\ n, k) = \frac{p^k (1-p)^{n-k}}{\beta\ (1,1)}$$

The expected probability, $\overline{p}$ and standard deviation, σ_{p_k} are

$$\overline{p}\ = \frac{k+1}{n+2}$$

$$\sigma_{p_k} = \frac{(k+1)(n-k+1)}{(n+2)^2(n+3)}$$

Thus, we can estimate the expected waiting time based on the expected probability and the standard deviation for the given simulation time derived from the number of opening events, *k*, observed in *n* simulations. The average waiting time, $1/\lambda$ and the standard deviation are calculated with the average probability, $\overline{p}$ and its standard deviation, σ_{p_k} for Extended Data Fig. 8B as below:

$$T_{wait} = \frac{1}{\lambda} = \frac{-Tm}{\ln(1-\overline{p})}$$

$$dT_{wait} = \frac{Tm}{(1-\overline{p})[\ln(1-\overline{p})\ ]^2}\ \sigma_{p_k}$$

Analysis of the Mg-dependent gate open and closed state durations arising from the salt-bridge switch model

Based on the Mg-dependent salt-bridge switch model (Fig. 5A and Extended Data Fig. 12), we calculate the open and closed time durations (τ_O and τ_C) from the transition rates between states in the kinetic scheme using a recursive relation [3,4]:

$$\tau_o = \frac{k_{on}\left(k_{off}+k_{on}+k_{close}\right)+k_{off}(k_{on}+k_{close})+k_{off}k_{close}}{k_{on}k_{off}k_{close}}$$

$$\tau_c = \frac{k_C k'_{on}\left(k'_{off}+k'_{on}+k_{op}\right)+k_C k'_{off}\left(k'_{on}+k_{op}\right)+k_C k'_{off}k_{op}+k_L\left(k'_{off}k'_{on}+k'_{off}k_{op}+k'_{off}k_{op}\right)+k'_{on}k'_{off}k_{op}}{k_c k'_{on}k'_{off}k_{op}}$$

To test the proposed kinetic model, we fit the experimentally determined Mg- dependent gate dynamics (Fig. 2F) to the derived expressions for the open and closed state lifetimes (Fig. 5C). The aim is to qualitatively reproduce the parabolic Mg-dependence rather than accurately determine all fit parameters, which would be difficult considering the number of kinetic parameters, particularly for τ_C.

To simplify the fitting and reduce the number of fitting parameters, we set k_c and k_L to be proportional to the magnesium concentration consistent with the ensemble measurement (Extended Data Fig. 2B). Additionally, we use the average $K_{L/C}$ from the ensemble measurements to relate k_c and k_L.

$$k_c = c([\mathrm{Mg}^{2+}])$$

$$k_L = < K_{L/C} > k_c$$

c was the only fit parameter related to the cleavage and religation rates. The other fit parameters are the Mg-binding (k_{on} and $k_{on}^{'}$) and unbinding (k_{off} and $k_{off}^{'}$) rates in the open and closed states, and the mechanical opening and closing rates, k_{open} and k_{close}, respectively.

Fitting parameters for the Mg-dependent τ_C and τ_O durations at a force of 5 pN:

τ_C		τ_O	
k'_{on}	310 $mM^{-1}s^{-1}$	k_{on}	0.7 mM^{-1} s^{-1}
k'_{off}	9.0 s^{-1}	k_{off}	0.8 s^{-1}
k_{open} (5 pN)	19.4 s^{-1}	k_{close} (5 pN)	1.6 s^{-1}
c	0.17 $mM^{-1}s^{-1}$		
$K_{d, Mg}$ (closed state)	29 μM	$K_{d, Mg}$ (open state)	1.1 mM

The high magnesium K_d values are consistent with weak Mg binding. The higher $K_{d, Mg}$ for the open state, $K_{d, Mg}$ (open state) suggests that the conformation of the open gate state renders Mg binding less favorable. Given the large uncertainties, simplifying assumptions, and simplified kinetic model, the fit displayed in Fig. 5C in the main text is primarily a demonstration that the kinetic scheme derived from the Mg-dependent salt-bridge model can quantitively describe the parabolic magnesium dependence of both the gate opening and closing rates with a single magnesium binding site. The actual fit parameters should be considered as estimates.

Table S1: list of DNA oligos and PCR templates that were used for generating substrates.

Coilable bubble DNA	
3kb biotin side left primer	GGGTCTCGCAACCTCAGTACAATCTGCTCTGATG
3kb biotin side right primer	GGGTCTCGCCCATCCGGATATAGTTCCTCCTTTC
3kb digoxigenin side left primer	GCTGGGTCTCGCCACTTAATCGCCGCGACAATTTGCGACG
3kb digoxigenin side right primer	GCTGGGTCTCGACCAACGCTCAAGTCAGAGGTGGCGAAAC
DNA bubble top	5′ phos-TGGGGCTTAGCTTAGAATCA TTTTTTTTTTTTTTTTTTTT TTTTT GCATCTAGACAGTGAC
DNA bubble bottom	5′ phos-GTGGGTCACTGTCTAGATGC GAT TTG GGA TGTTGATTCTAAG CTAAGC
PCR template	pKZ1
Gapped DNA	
438 bp for primer	GCTGGGTCTCGACCACGGATATAGTTCCTCCTTTC
438 bp rev primer	GCTGGGTCTCGCAACTTGTGAGCGGATAACAATTC
Gapping oligo	GGCGCAGCTTCCGACTGCAGCCTGACGCCAGGGCTGA
PCR template	pKZ1
579 bp DNA hairpin	
DNA hairpin dig-handle side primer	GCTGGGTCTCGACCA CGGATATAGTTCCTCCTTTC
DNA hairpin T-loop side primer	GCTGGGTCTCGCAACGCGAAAGGTTTTGCGCCATTCG
T-loop	5′ phos-GTTGCATGGCAGTAGGTTTTCCTACTGCCATG
3′Bio polydT40	5′ phos-TCAGCCCTGGCGTCAGGCTGCAGTCGGAAGCTG-poly T (40)
PCR template	pKZ1
Multi-bio or dig labelled DNA handles	
Multi-biotinylated handle primer	GCTGGGTCTCGGTTGTTCCCTTTAGTGAGGGTTAATTG
Multi-digoxigenin handle primer	GCTGGGTCTCGTGGTTTCCCTTTAGTGAGGGTTAATTG
Reverse primer	TATAGTCCTGTCGGGTTTCG (500 bp) GAGTTAGCTCACTCATTAGGCACCC (166 bp)
PCR template	pKZ1

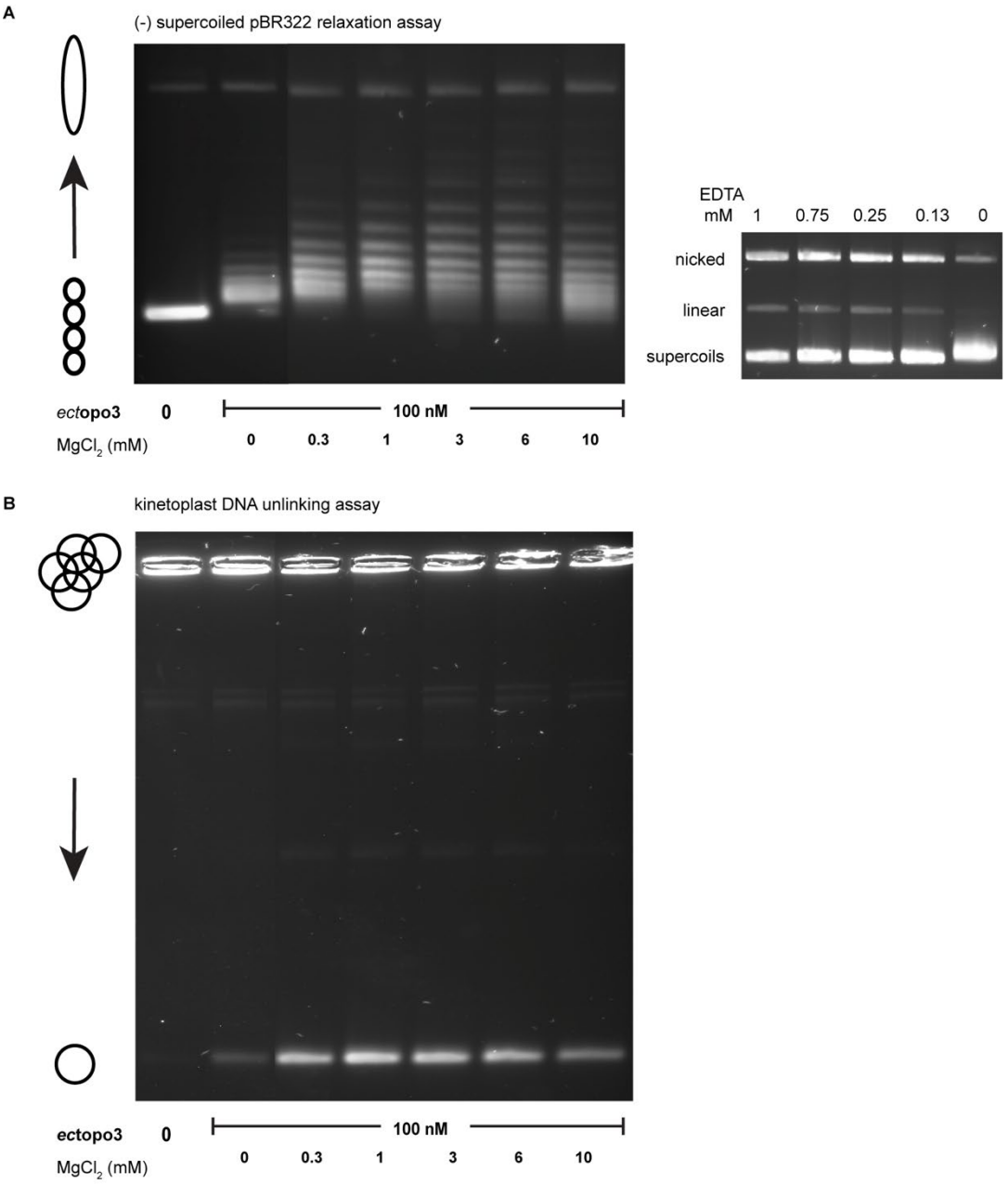

Extended Data Fig. 1. **A.** Example agarose gel (1%) displaying *ec*topo3 relaxation of negatively supercoiled plasmid DNA as a function of Mg concentration (methods). Inset: titrating EDTA to determine the concentration required to deplete divalent metal ions (1 mM) as evidenced by the lack of relaxation. **B.** Example agarose gel (1%) displaying *ec*topo3 decatenation of kDNA as a function of magnesium concentration. We note that supercoil relaxation and unlinking activity were detected without the addition of magnesium to the reaction ($MgCl_2$=0). This is likely due to trace magnesium or other divalent metal ions present in the buffer. Catalytic activity, but not DNA cleavage, was inhibited by 1 mM EDTA that chelates Mg^{2+}.

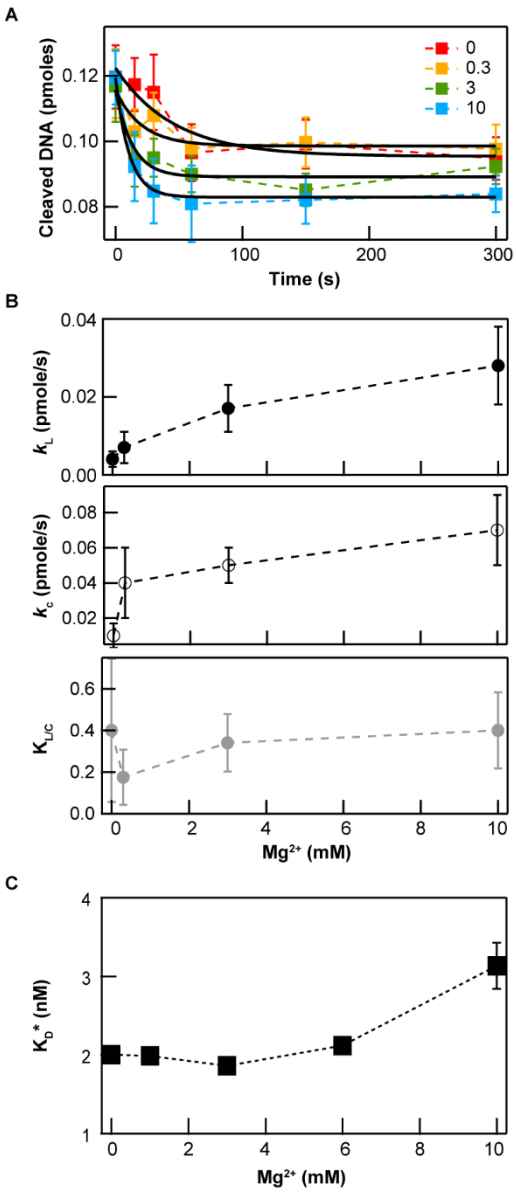

Extended Data Fig. 2. Ensemble measurement of *ec*topo3 religation-cleavage equilibrium. **A.** The amount of cleaved DNA substrate over time as a function of Mg^{2+} concentration (markers correspond to Mg^{2+} concentration from 0 to 10 mM) fit with eq. s1 (supplementary information). The error bars correspond to SEM (N=5). **B.** The effective ligation and cleavage rates (k_L and k_c, respectively) in addition to the religation-cleavage equilibrium ($K_{L/c}$) as a function of Mg^{2+} for *ec*topo3 obtained from the fits to the data in panel A**.** Both k_L and k_C increased monotonically with Mg^{2+} concentration above 0 mM. On the other hand, $K_{L/c}$ remained largely independent of Mg^{2+}. The error bars correspond to fitting errors. **C.** Single-stranded DNA binding affinity of *ec*topo3 as a function of Mg^{2+} concentration (Supplementary information). The error bars correspond to SEM (N=3).

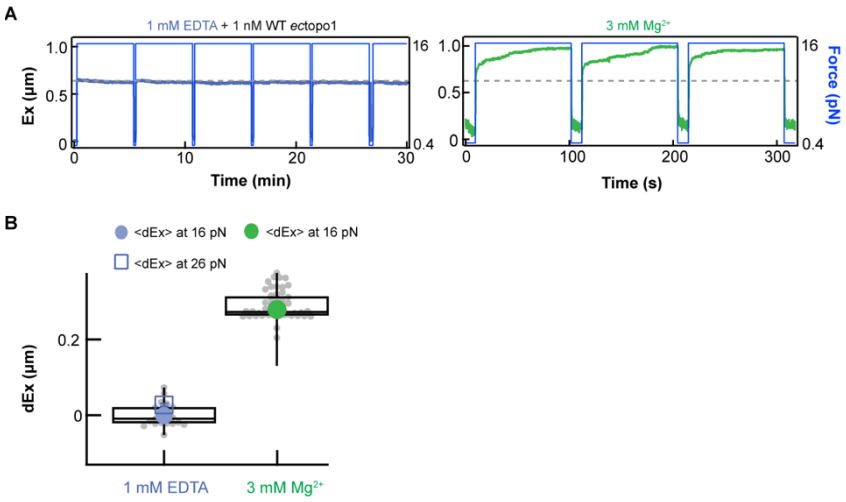

Extended Data Fig. 3: **Full gate opening of *ec*topo1 requires magnesium**. **A.** Example trace of *ec*topo1 gate opening measurement at 1 mM EDTA showed no change of DNA extension, indicating no gate-opening (left panel). After removing 1 mM EDTA and unbound enzymes followed by introducing protein-free buffer with 3 mM Mg^{2+}, the DNA extension increased, indicating gate-opening. **B.** Box plots of extension change (dEx) at 1 mM EDTA and 3 mM Mg^{2+} (gray points and solid lines). The corresponding averages of dEx, <dEx> at 1 mM EDTA under 16 pN and 26 pN (blue filled circle and blue open square, respectively) and at 3 mM Mg^{2+} under 16 pN (green filled circle) are overlayed on the box plots. Number of DNA molecules: 2.

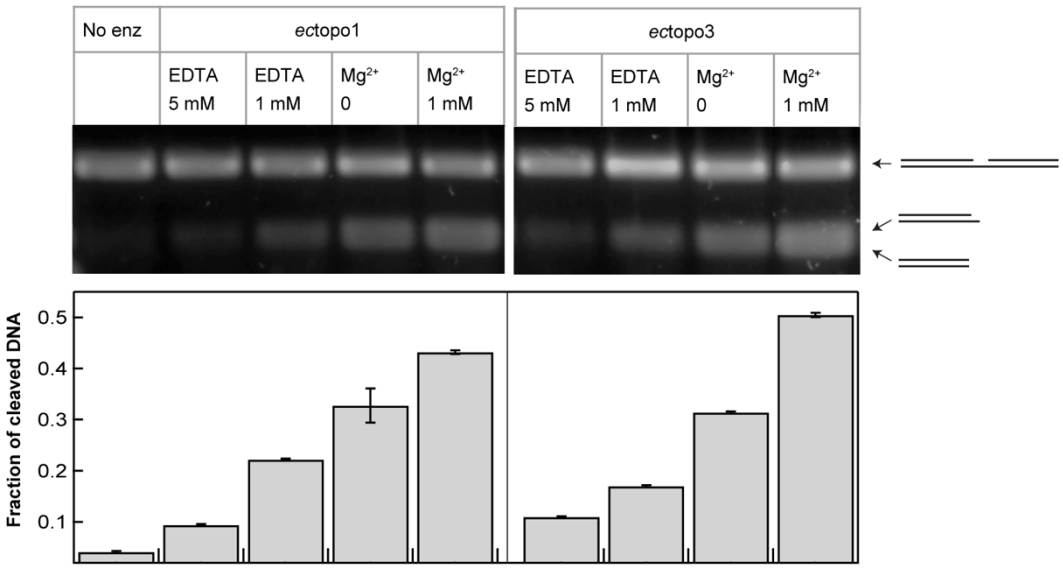

Extended Data Fig. 4: **Ensemble cleavage of the gapped DNA substrate used in the single-molecule TopIA gate dynamics measurements**. Both *ec*TopIA cleaved gapped DNA substrates under different conditions (30 minute incubation). The ensemble cleavage reactions were visualized on a 2% agarose gel (top). The quantitative fractions of cleaved DNA corresponding to each gel lane are shown below the gel.

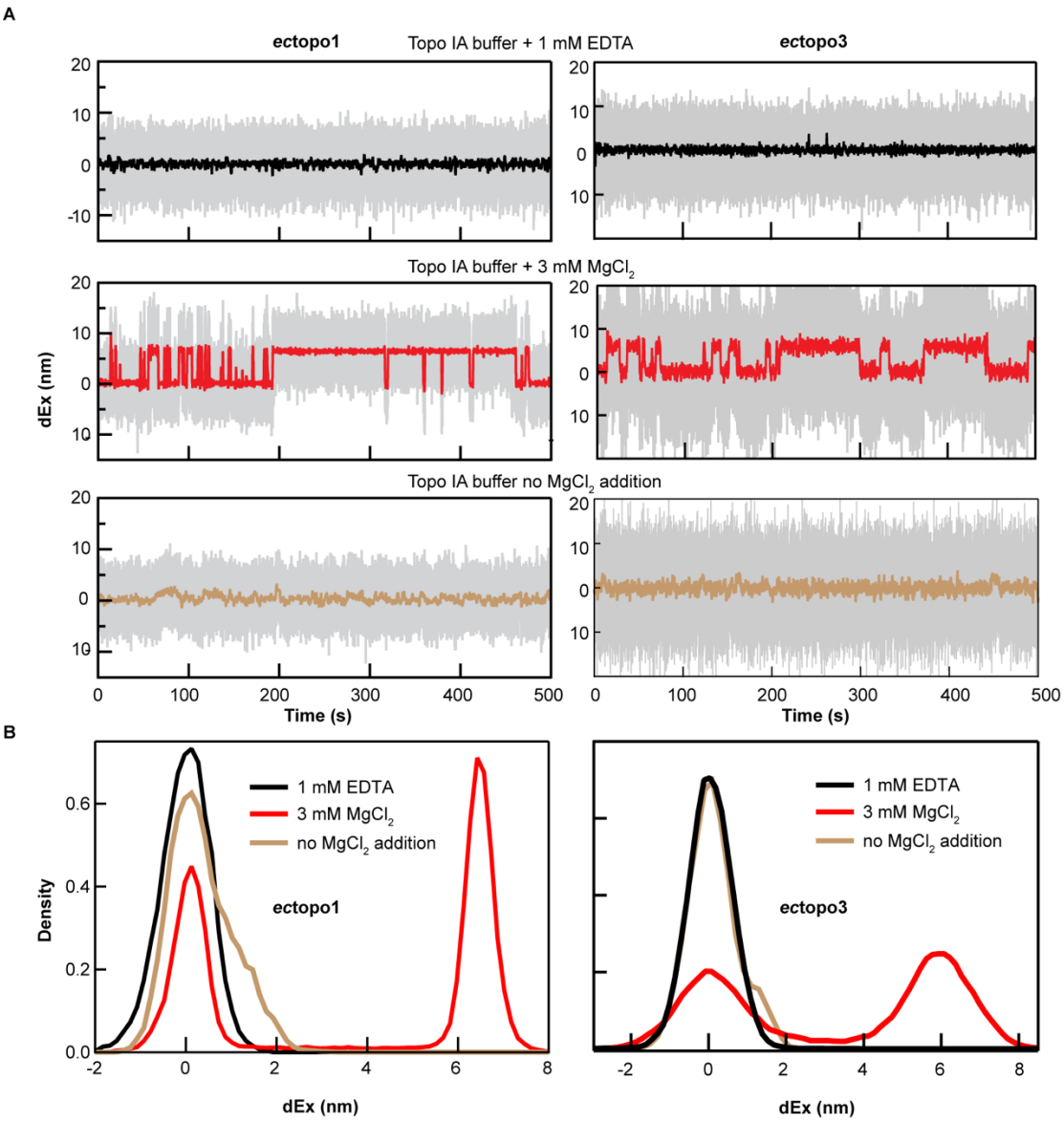

Extended Data Fig. 5. Both *ec*topo1 and *ec*topo3 require Mg^{2+} for complete gate opening and dynamics. A. Example traces with buffer supplemented with 1 mM EDTA, 3 mM Mg^{2+}, or in the absence of Mg^{2+}. **Top.** No visible extension changes were observed for either topIA enzyme under Mg depletion conditions (1 mM EDTA). **Middle.** ~6 nm extension fluctuations associated with gate dynamics were observed for both TopIA enzymes in the presence of Mg. **Bottom.** Occasional small fluctuations (1-2 nm) were observed without added Mg^{2+}. **B.** The probability density distributions of the example traces shown in **A**.

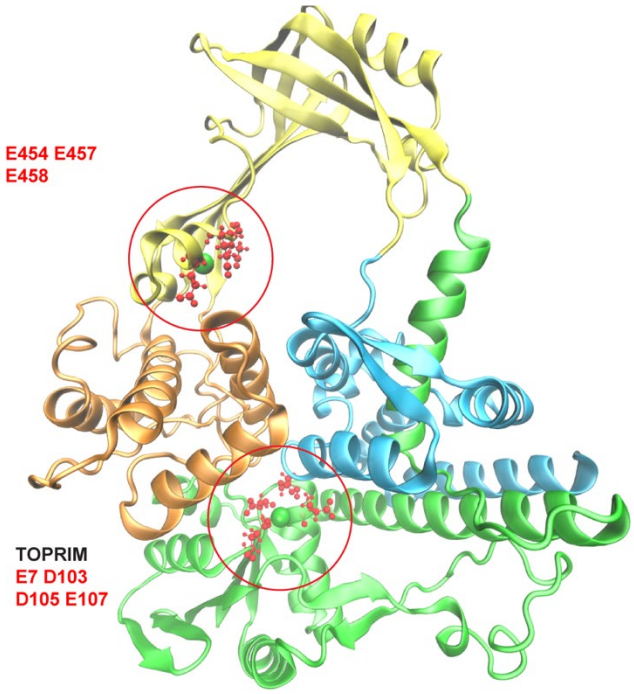

Extended Data Fig. 6. Divalent metal binding site formed by the acidic triad: E454, E457, and E458 predicated by BioMetAll [5]. The conserved magnesium binding site within the TOPRIM domain was also predicted as a potential divalent metal binding site. The bound metal ions are indicated as green spheres and the residues forming the acidic triads are represented in red ball and stick configurations. The structure of *ec*topo3 was obtained via homology modelling based on PDB 2O19 [6,7].

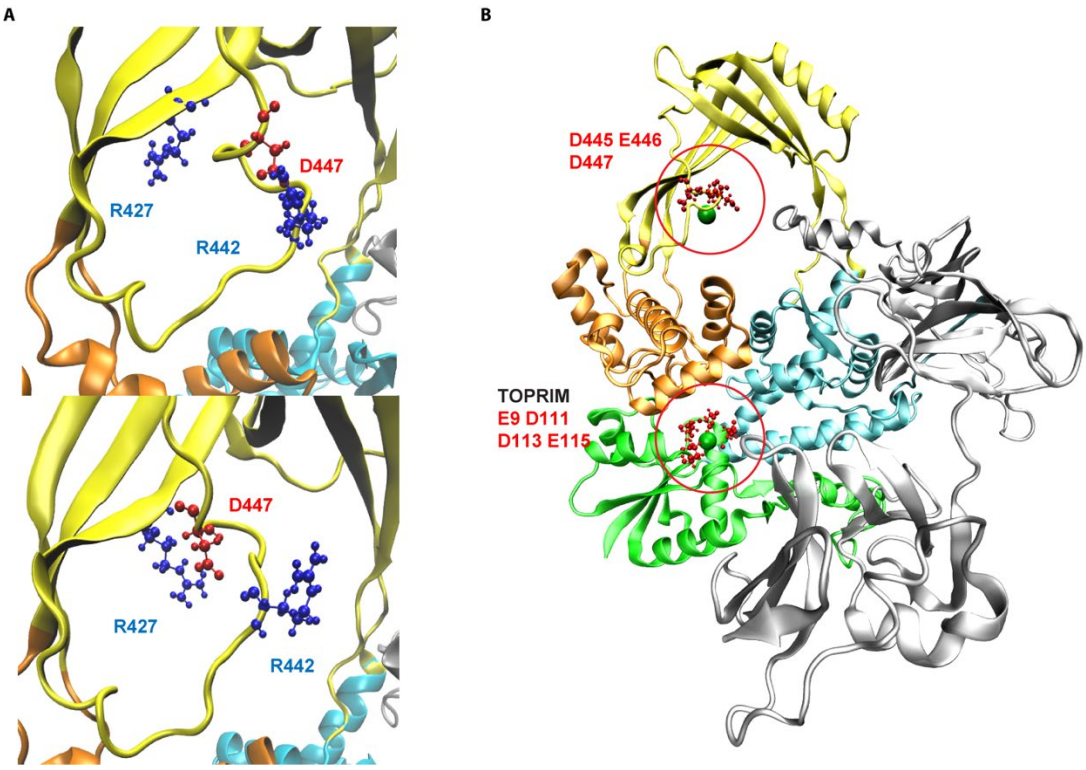

Extended Data Fig. 7. *ec*topo1 and *ec*topo3 share a similar divalent metal binding site that overlaps competing inter- and intra-domain salt bridges.. **A.** The structure of *ec*topo1 was obtained via homology modelling based on PDB 4RUL[6,8]. In *ec*topo1, the acidic residue D447 can form a salt-bridge with R442 (top) or with R427 (bottom) that can influence domain III movement in an analogous manner as in *ec*topo3. **B.** The acidic triad including residue D447 was predicted as a potential Mg binding site by BioMetAll[5]. The conserved magnesium binding domain, TOPRIM (E9, D111, D113, and E115) was also predicted as a potential metal binding site for *ec*topo1. Bound metal ions are indicated as green spheres and the residues forming the acidic triads are represented in red ball and stick configurations. Despite the overall similarities in the divalent metal binding and competing salt bridge topology between *ec*topo1 and *ec*topo3, the residues and the structural arrangement in *ec*topo1 differ slightly from those of *ec*topo3. In contrast to the interdomain salt-bridge (domain II-III) that likely hinders full opening of the protein-gate in *ec*topo3, *ec*topo1 residue D447, part of the Mg binding acidic triad, interacts with R442, promoting bending of the β sheet linked to domain III, possibly leading to a partial opening of the protein-gate. Divalent metal binding at the acidic triad (445-447) could promote switching of the D447 salt bridge from R442 to R427 in a similar manner as proposed for *ec*topo3.

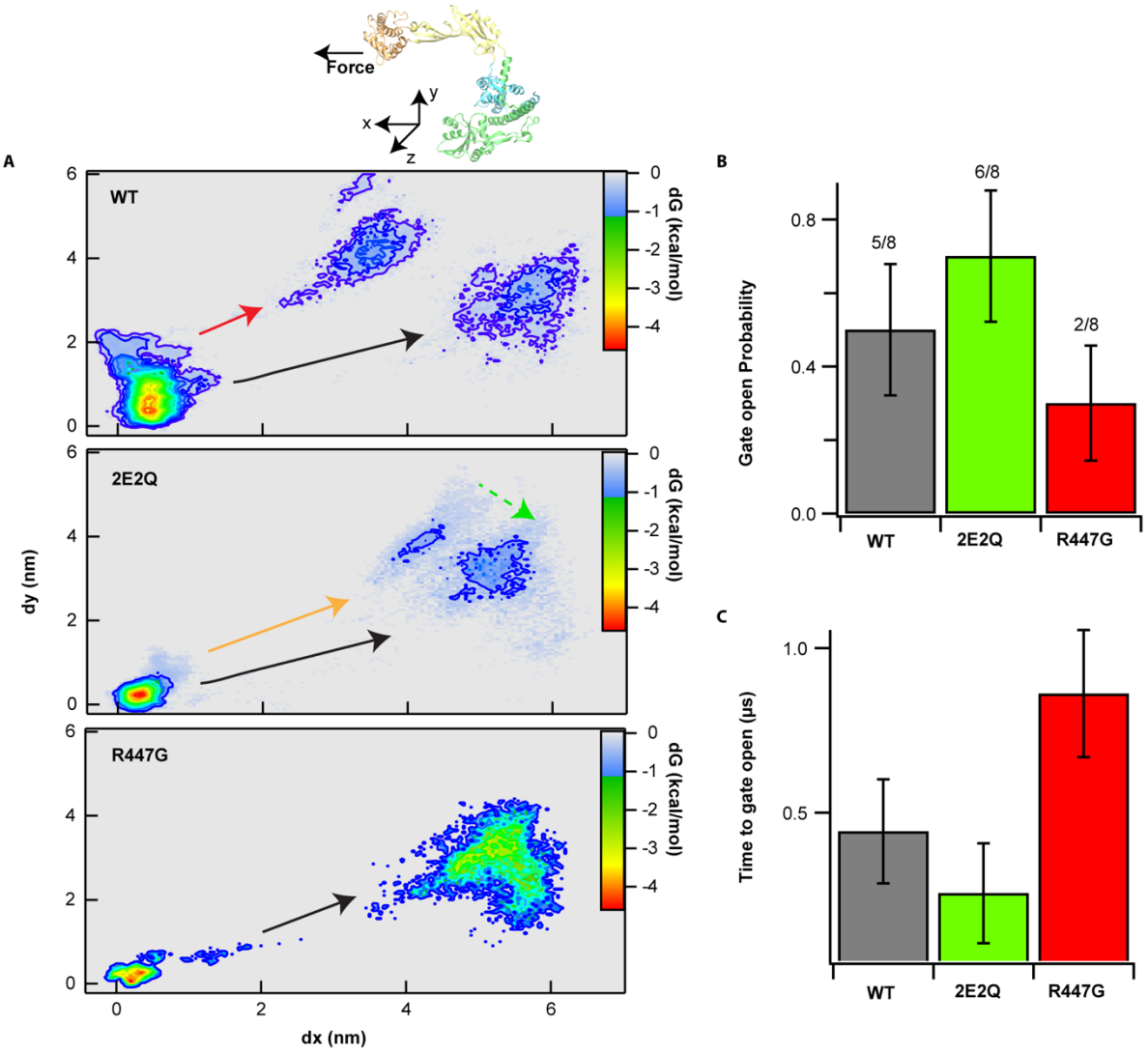

Extended Data Fig. 8. Constant force SMD with 2E2Q and R447G salt-bridge variants compared to WT *ec*topo3. A. 2-dimensional average energy landscapes of gate opening transitions for the three *ec*topo3 variants (obtained from 8 trajectories for each variant). The *x*- and *y*- axes correspond to the center of mass motion of the catalytic tyrosine in domain III parallel and orthogonal to the direction of applied force, respectively (inset). WT showed two distinctive transition pathways as discussed in Fig. 2A. The black arrow indicates a transition pathway similar to ″Sim1″, typified by rapid gate opening without intermediates. The red arrow corresponds to a transition pathway similar to ″Sim2″, which includes intermediate states without full gate opening. The 2E2Q trajectories did not exhibit a stable intermediate state preceding opening in contrast to WT, but some trajectories exhibited a slight orthogonal component leading to two different open states (black and orange arrows). The open state indicated by the orange arrow, which exhibited slightly less parallel and more orthogonal displacement, eventually converged to the other open state (green arrow). The R447G gate opening trajectories show the least orthogonal motion indicating that transient interactions between R447 and the acidic triad (454, 457, and 458) are likely responsible for orthogonal movement of domain III. **B.** Gate opening transition probabilities for the three *ec*topo3 variants for 300 ns simulations (*N*= 8 trajectories for each enzyme). The average probabilities and the standard deviations were calculated based on Bayesian inference of the finite-duration simulation trajectories (Supplementary information)**. C.** Expected waiting times before gate opening. The waiting times were estimated based on the probability estimates from B given the 300 ns simulation time (Supplementary information). The error bars correspond to the SEM.

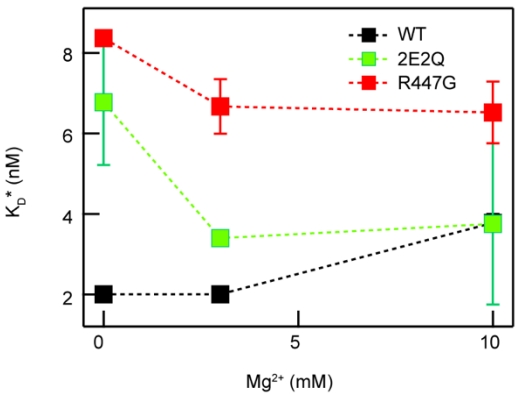

Extended Data Fig. 9. Single-stranded DNA binding affinity of WT, 2E2Q, and R447G as a function of Mg^{2+} concentration. Apparent K_d (K_d*) as a function of Mg concentration for the three *ec*topo3 variants determined from fluorescence anisotropy measurements. Error bars correspond to the standard deviation (SD) of three measurements.

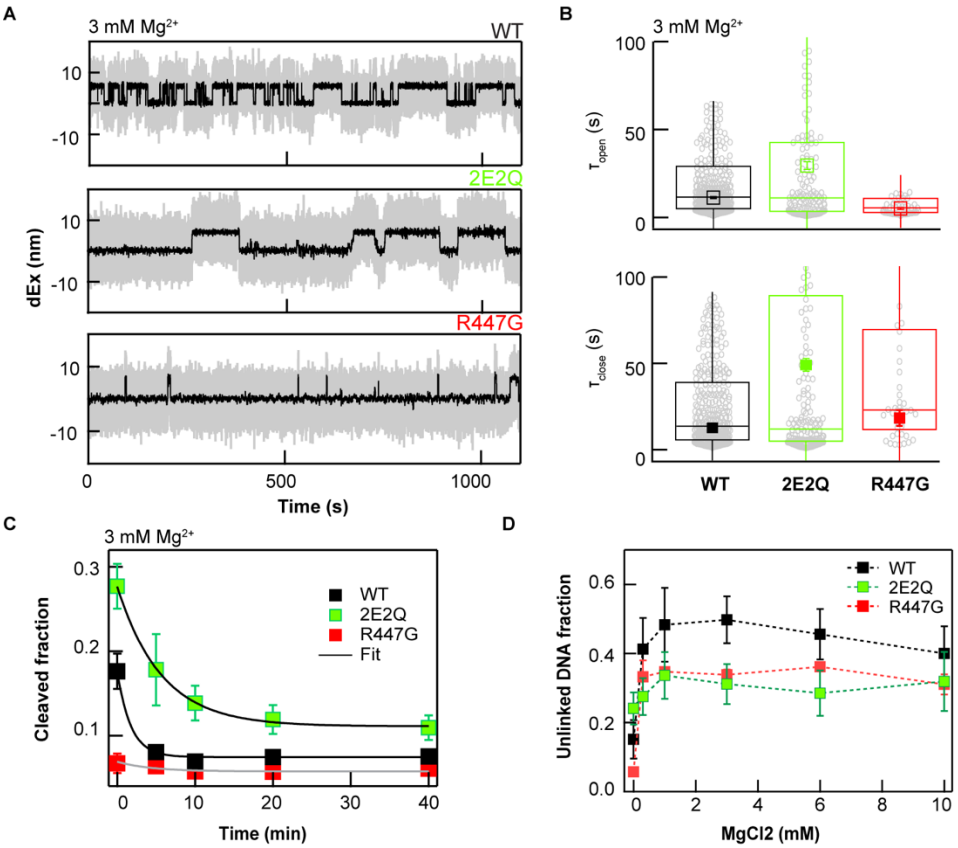

Extended Data Fig. 10. Salt-bridge mutations adversely affect Mg^{2+}-dependent topo3 catalytic activities. A. Gate dynamics trajectories of three *ec*topo3 variants at 3 mM Mg^{2+}. All three enzymes show full gate opening. However, 2E2Q gate opening exhibited a mixture of fast (comparable to WT) and slow dynamics whereas R447G displayed overall slower gate dynamics than WT. **B.** Box plots of open and closed state durations for the three variants. The horizontal lines within the boxes indicate the median, whereas the overlayed rectangles indicate the average value from single exponential fits with standard deviations as errors. 2E2Q gate open and closed durations are broadly distributed, reflecting the mixture of fast and slow gate dynamics shown in **A**. Number of molecules: 8 (WT); 5 (2E2Q); 5 (R447G). **C.** Cleaved DNA fraction as a function of time for three *ec*topo3 variants fit with a cleavage-religation equilibrium function (Supplementary information). R447G data was omitted from the analysis due to insufficient cleaved DNA. The rate of reduction in the cleaved fraction reflects religation and cleavage rates. **D.** Decatenation activities of the three variants as a function of Mg concentration. Deregulation of gate dynamics in 2E2Q adversely affects enzyme catalytic activity by reducing cleavage and religation rates resulting in inefficient decatenation. Furthermore, lower decatenation activity of R447G relative to WT indicates that Mg^{2+} alone was insufficient to fully compensate for the role of R447 in destabilizing the closed state. Number of events: 5 (WT); 6 (2E2Q); 3 (R447G). Error bars indicate the standard error of the mean.

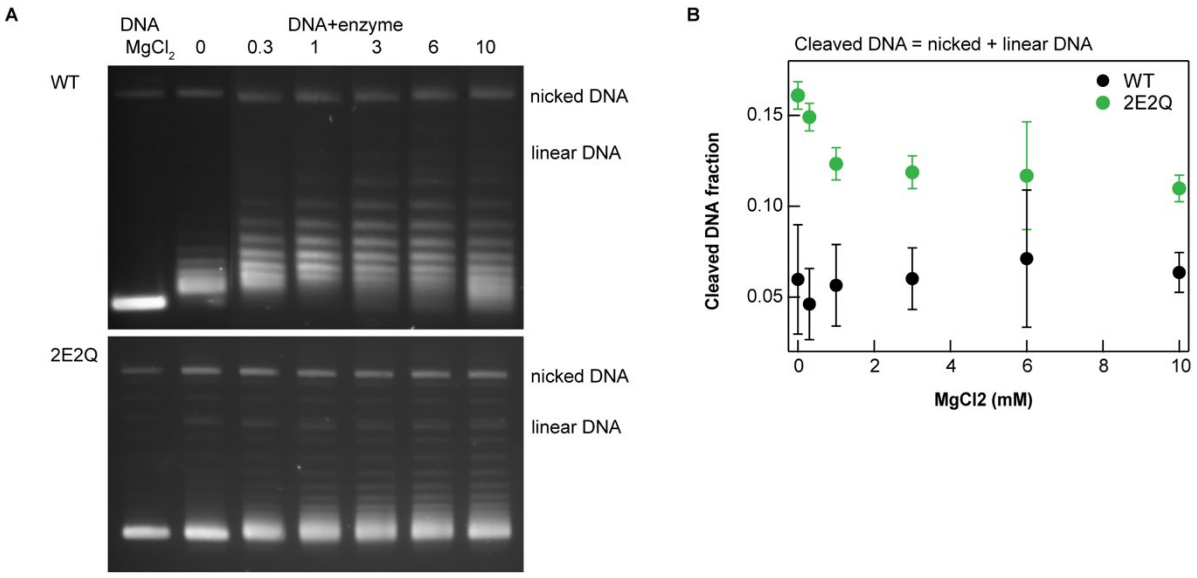

Extended Data Fig. 11. 2E2Q exhibits higher level of DNA cleavage compared to WT. A. DNA supercoil relaxation measurements of WT and 2E2Q visualized by agarose gel electrophoresis. 2E2Q showed a higher propensity for cleavage as evidenced by the higher fraction of nicked and linear bands in comparison to WT *ec*topo3. **B.** Cleaved DNA fraction as a function of Mg concentration obtained from analysis of the gels in panel **A**.

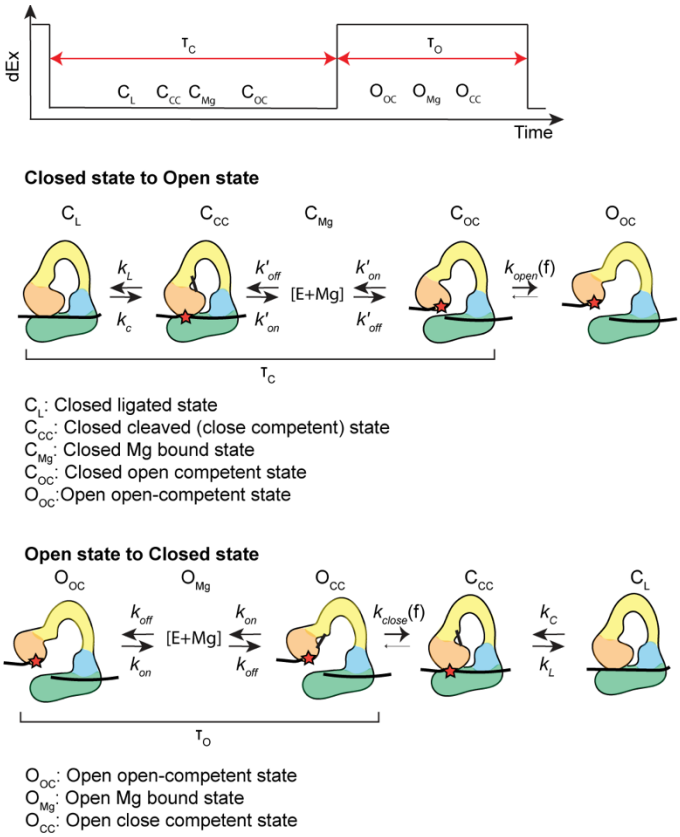

Extended Data Fig. 12. Mg-dependent salt-bridge switch kinetic model. The experimentally observed gate motion was modeled as a two-state telegraphic signal in which the lower signal represents the closed state, and the higher signal represents the open state. The open and closed state lifetimes are each comprised of several sequential rates. Expressions for the open and closed state lifetimes based on this kinetic scheme are described above.

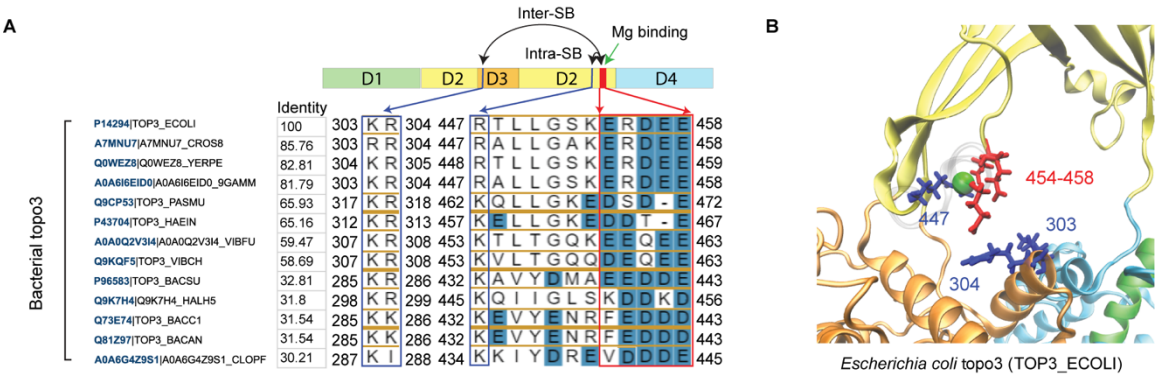

Extended Data Fig. 13. Sequence conservation of overlapping salt-bridge and magnesium binding site architecture among bacterial topoisomerase 3 enzymes. A. Sequence alignment of bacterial topo3 revealed that the Mg binding-site residues (red lines and outlines) and inter- and intra-domain salt-bridge forming residues (blue lines and outlines) are highly conserved, suggesting that they share the same Mg-dependent protein gate regulation. **B.** Representative structure of E. *coli* topo3 indicates the arrangement of the two basic residues and multiple acidic residues involved in inter- and intra-domain salt-bridges and Mg binding. Green sphere indicates a magnesium ion. The structure of *ec*topo3 was obtained via homology modelling based on PDB 2O19. [6,7]

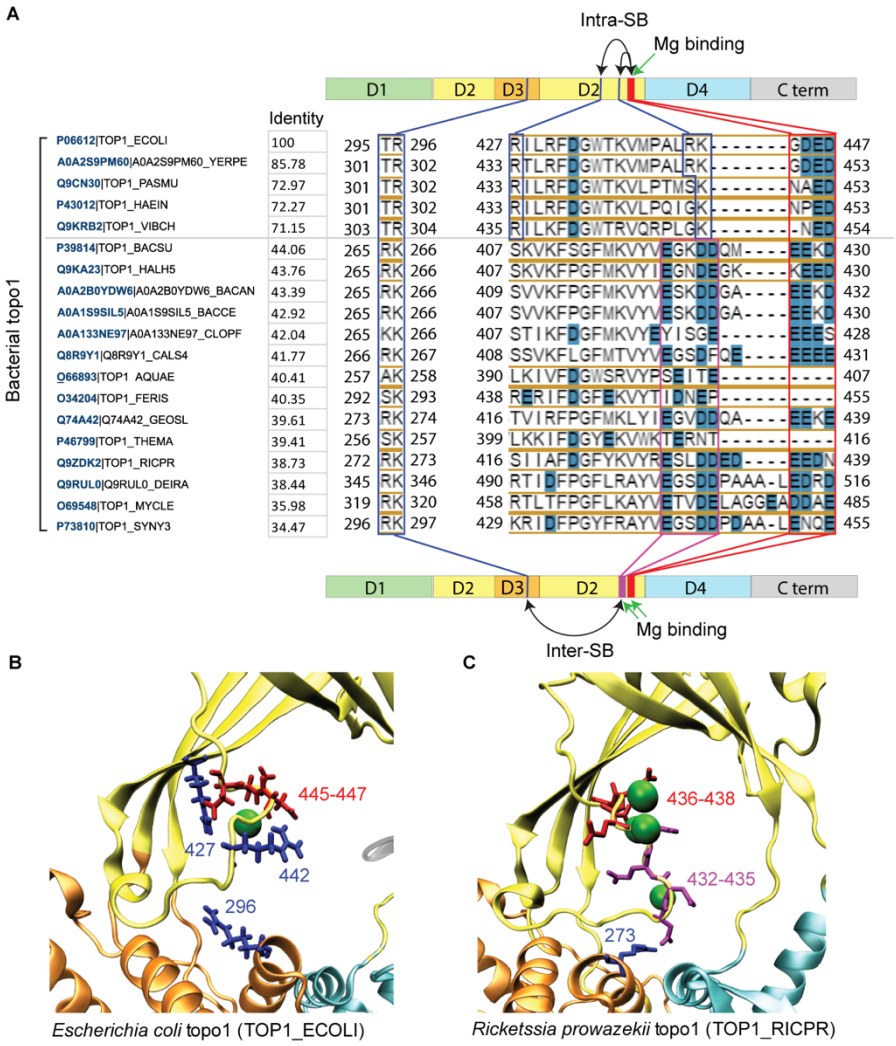

Extended Data Fig. 14. Sequence and putative functional conservation of salt-bridge and Mg binding site architecture among bacterial topoisomerase 1 enzymes. A. Sequence alignment of bacterial topo1 showed that enzymes closely related to *E. coli* topo1 (identity >70%) have a similar arrangement of the salt-bridge forming (blue lines and outlines) and Mg binding residues (red lines and outlines) in domain II, whereas those with lower identities possess an inter-domain salt-bridge arrangement similar to *ec*topo3 (Extended Data Fig. 13) with an additional acidic residue patch (magenta) in domain II. The multiple acidic regions (magenta and red) possibly accommodate multiple magnesium ions. **B.** Representative structure of *E. coli* topo1 indicates the arrangement of the two basic residues and multiple acidic residues involved in the intra-domain salt-bridge and Mg binding. Green sphere indicates magnesium. The structure of *ec*topo1 was obtained via homology modelling based on PDB 4RUL [6,8]. **C.** Representative structure of *Ricketssia prowazekii* topo1 from the AlphaFold protein structure database[9] as an example of the alternative sequence and architecture. Green spheres indicate magnesium ions.

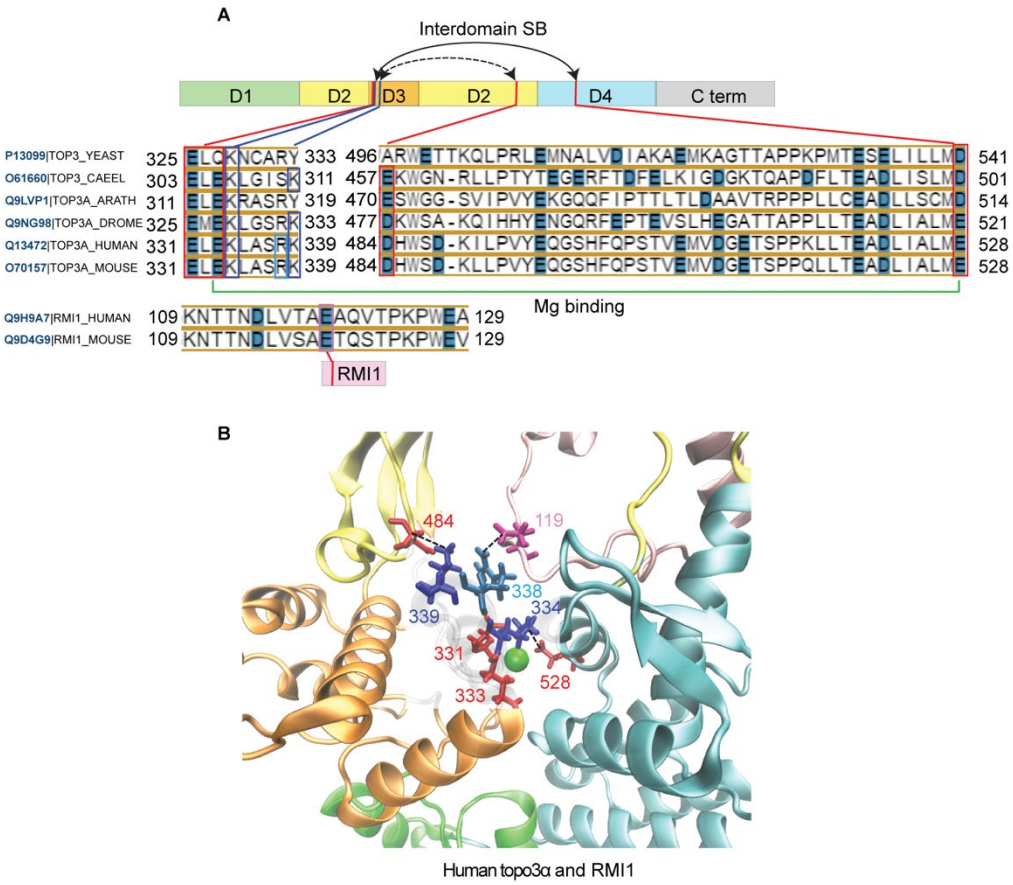

Extended Data Fig. 15. Functional conservation of Salt-bridge and Mg binding site architecture in human topoisomerase 3α-RMI1 complex. A. Sequence alignment of multiple eukaryotic topo3 revealed residues that could functionally replicate the Mg-dependent protein gate regulation though alterations in salt-bridge topology. **B.** The conserved residues contributing to the putative Mg-dependent salt-bridge architecture in **A** and a divalent metal (green sphere) are indicated in the expanded view of human topoisomerase 3α (htopo3α) and RMI1 complex structure (based on PDB 4CGY). The salt-bridge interaction between K334 (Domain 3) and E528 (Domain 4) hinders gate-opening that can be disrupted by Mg binding coordinated by (E331, E333, and E528). One of the conserved basic residues in domain III of htopo3α (K339) maintains an inter-domain salt-bridge with D484, while the other residue (R338) interacts with an acidic residue (E119) in the RMI1 insertion loop [10].

References

1 Schindelin, J. *et al.* Fiji: an open-source platform for biological-image analysis. *Nature Methods* **9**, 676-682 (2012). https://doi.org:10.1038/nmeth.2019

2 Donovan, T. & Mickey, R. M. *Bayesian Statistics for Beginners: a step-by-step approach*. (Oxford University Press, 2019).

3 Seol, Y., Zhang, H., Pommier, Y. & Neuman, K. C. A kinetic clutch governs religation by type IB topoisomerases and determines camptothecin sensitivity. *Proceedings of the National Academy of Sciences of the United States of America* **109**, 16125-16130 (2012). https://doi.org:10.1073/pnas.1206480109

4 Shaevitz, J. W., Block, S. M. & Schnitzer, M. J. Statistical Kinetics of Macromolecular Dynamics. *Biophysical Journal* **89**, 2277-2285 (2005). https://doi.org:https://doi.org/10.1529/biophysj.105.064295

5 Sánchez-Aparicio, J.-E. *et al.* BioMetAll: Identifying Metal-Binding Sites in Proteins from Backbone Preorganization. *Journal of Chemical Information and Modeling* **61**, 311-323 (2021). https://doi.org:10.1021/acs.jcim.0c00827

6 Waterhouse, A. *et al.* SWISS-MODEL: homology modelling of protein structures and complexes. *Nucleic Acids Res* **46**, W296-w303 (2018). https://doi.org:10.1093/nar/gky427

7 Changela, A., DiGate, R. J. & Mondragón, A. Structural Studies of E. coli Topoisomerase III-DNA Complexes Reveal A Novel Type IA Topoisomerase-DNA Conformational Intermediate. *Journal of molecular biology* **368**, 105-118 (2007). https://doi.org:10.1016/j.jmb.2007.01.065

8 Tan, K. *et al.* Structural basis for suppression of hypernegative DNA supercoiling by E. coli topoisomerase I. *Nucleic Acids Research* **43**, 11031-11046 (2015). https://doi.org:10.1093/nar/gkv1073

9 Varadi, M. *et al.* AlphaFold Protein Structure Database in 2024: providing structure coverage for over 214 million protein sequences. *Nucleic Acids Research* **52**, D368-D375 (2023). https://doi.org:10.1093/nar/gkad1011

10 Bocquet, N. *et al.* Structural and mechanistic insight into Holliday-junction dissolution by Topoisomerase IIIα and RMI1. *Nature Structural & Molecular Biology* **21**, 261-268 (2014). https://doi.org:10.1038/nsmb.2775